




Cite this: *RSC Adv.*, 2017, 7, 52626

Mesoporous silica-based carbon dot–carbon nitride composite for efficient photocatalysis†

Yulan Peng,^a Fenghui Liu,^a Lingzhi Wang,^a ^a Yongdi Liu,^b Juying Lei ^{*b} and Jinlong Zhang ^{*a}

In this work, graphene carbon nitride (g-C₃N₄, CN) is loaded into the carbon dots (CD) modified SBA-15 mesoporous silica by a precursor impregnation method. The obtained samples are characterized by various spectroscopy techniques and applied in the visible-light-driven photocatalytic degradation of phenol. The photocatalytic activity of the obtained SBA15–CN is 2 times as high as that of pure g-C₃N₄ due to the high dispersion of g-C₃N₄ into SBA-15 channels. For CD-SBA15–CN, the visible light driven photocatalytic activity is further increased, which is 4 times as high as that of pure g-C₃N₄. This promotion can be attributed to carbon dots with the ability to transfer photogenerated electrons as well as the compound catalyst having a bigger surface area and pore volume. When the weight ratio of CD-SBA15/g-C₃N₄ was 1 : 6, the catalyst (1 : 6 CD-SBA15–CN) performed best. The 1 : 6 CD-SBA15–CN photocatalyst had enhanced visible absorption and the interaction between CDs and g-C₃N₄ can further promote the separation of photo-generated electrons and holes, achieving the highest photocatalytic activity of CD-SBA15–CN compared to SBA15–CN and g-C₃N₄.

Received 14th August 2017
Accepted 23rd October 2017

DOI: 10.1039/c7ra08969d

rsc.li/rsc-advances

1. Introduction

The degradation of organic pollutants in water and the production of H₂ or O₂ from water by using semiconductor-based photocatalysts have attracted great attention because of the global environment pollution and energy crisis.^{1,2} To date, various efficient photocatalysts have been developed, such as TiO₂,^{3,4} CdS,^{5,6} and so on. In particular, g-C₃N₄ as a novel organic semiconductor with a special layered structure, has been considered to be a fascinating candidate for photocatalysis due to its unique properties.^{7,8} In 2009, Wang *et al.* first reported the excellent photocatalytic ability of g-C₃N₄ for hydrogen production.⁹ Since then, the photocatalytic performance of g-C₃N₄ for degradation of organic pollutants in wastewater has also been investigated.^{10,11}

However, the photocatalytic efficiency of g-C₃N₄ is relatively low, mainly due to the small surface area, quick recombination of photo-generated electron–hole pairs and limited visible light utilization.¹² In order to address these problems, a variety of methods have been developed such as morphology control,^{13,14}

element doping,¹⁵ coupling with other semiconductor,^{16,17} and modification with carbon materials.¹⁸ Zhang *et al.* reported the carbon dots decorated g-C₃N₄ nanosheet and demonstrated that the composite catalyst had superior visible light photocatalytic activity as compared to pure g-C₃N₄.¹⁸

Meanwhile, mesoporous silica with high specific surface area can act as good host for semiconductor photocatalysts, leading to greatly improved photocatalytic performance by reducing the recombination of photo-generated electron–hole pairs in these semiconductors. Guo *et al.* discovered a CdS@Ti-MCM-41 composite with much higher visible light photocatalytic activity than the bulk CdS for hydrogen production from water.¹⁹ Li *et al.* dispersed nanophase g-C₃N₄ into SBA-15 by a two-step vapor-deposition method. The obtained materials are active catalysts for CO₂ activation and conversion.²⁰ In addition, in our previous work, mesoporous silica materials embedded with amide-containing carbon dots (CD) have been developed.²¹ Inspired by these works, we envision that CD modified SBA15-supported g-C₃N₄ materials will demonstrate higher photocatalytic performance than g-C₃N₄.

Herein, we report a facial route for the fabrication of CD-SBA15-supported g-C₃N₄ materials. When g-C₃N₄ is loaded into SBA-15, obtained SBA15–CN shows better visible-light photocatalytic activity than pure g-C₃N₄. In addition, the photocatalytic efficiency for degradation of phenol is further improved for CD-SBA15–CN. The mechanism for the enhanced photocatalytic activity has also been discussed.

^aKey Lab for Advanced Materials and Institute of Fine Chemicals, School of Chemistry and Molecular Engineering, East China University of Science and Technology, 130 Meilong Road, Shanghai 200237, P. R. China. E-mail: jlzhang@ecust.edu.cn

^bState Environmental Protection Key Laboratory of Environmental Risk Assessment and Control on Chemical Process, School of Resources and Environmental Engineering, East China University of Science and Technology, 130 Meilong Road, Shanghai 200237, P. R. China. E-mail: lejuying@ecust.edu.cn

† Electronic supplementary information (ESI) available. See DOI: 10.1039/c7ra08969d



2. Experimental

2.1 Chemicals

Citric acid (CA), hexane, hydrochloric acid, tetraethoxysilane, melamine, phenol are all obtained from Shanghai Ling Feng Chemical Reagent Co, Ltd. Pluronic P123, *N*-(β -aminoethyl)- γ -aminopropylmethyldimethoxysilane (AEAPMS) are purchased from Aldrich reagent plant. The reagents are all used as received from the suppliers without further purification. And deionized water is used for all solution experiments.

2.2 Preparation of silylated carbon dots (Si-CDs)

Si-CDs are prepared through a one-step synthetic procedure according to a method reported previously.^{22–25} The reaction proceeds through pyrolysis of anhydrous CA. 10 mL of AEAPMS is put in a three-necked flask with 50 mL of volume and the temperature is raised to 240 °C with stirring under N₂ atmosphere. Then 0.5 g of CA is quickly added into the flask. The heating is stopped after 1 minute reaction. When the reaction mixture is cooled to room temperature, it is washed twice using hexane, after which the oily liquid product is obtained. Then the product is sealed with hexane and stored for use in refrigerator.

2.3 Preparation of the CD incorporated SBA-15 mesoporous silica (CD-SBA15)

SBA-15 is prepared with Pluronic P123 as template *via* a method similar to previous report.²⁶ Then, an amount of CDs and SBA-15 are refluxed in dehydrated toluene (250 mL) at 110 °C for 24 h under N₂ flow. The obtained products are washed for three times with deionized water and dried over night at 60 °C. The resultant sample is denoted as CD-SBA15.

2.4 Preparation of g-C₃N₄ and CD-SBA15-CN

Pure g-C₃N₄ is prepared by the pyrolysis method. 4 g of melamine are put into a porcelain ark, heated to 520 °C in argon gas with a heating rate of 2 °C min⁻¹ and then maintained at 520 °C for 4 h.

The CD-SBA15-CN photocatalysts are prepared by calcining mixed CD-SBA15 and melamine in argon gas. In details, desired amounts of CD-SBA15 and melamine are put into 200 mL of deionized water at 90 °C and vigorously stirred for 2 h. Then the temperature is raised to 100 °C for evaporating the water. The obtained powder mixture of CD-SBA15 and melamine is collected and heated to 520 °C in argon gas with a heating rate of 2 °C min⁻¹ and then maintained at 520 °C for 4 h to get the final product. By this method, samples using mass ratio of CD-SBA15 to melamine of 1 : 1, 1 : 2, 1 : 4, 1 : 6 and 1 : 8 are prepared, and denoted as 1 : *x* CD-SBA15-CN (*x* = 2, 4, 6, 8), respectively. The reference sample of SBA15-CN is prepared by the same method using SBA-15 instead of CD-SBA-15 and the mass ratio of SBA15 to melamine is 1 : 6.

2.5 Characterizations

The morphology of the obtained CD-SBA15-CN series samples are observed by transmission electron microscopy (TEM,

JEM2000EX). The crystal structure of the samples are characterized by powder X-ray diffraction (XRD), which are recorded on a Rigaku D/MAX-2550 diffract meter using Cu K α radiation of wavelength 1.5406 Å, typically running at a voltage of 40 kV and current of 100 mA. UV-visible absorbance spectra are achieved for the dry-pressed disk samples using a Scan UV-visible spectrophotometer (SHIMADZU, uv-2450), and using BaSO₄ as a reflectance sample. BET surface area measurements are carried out by N₂ adsorption at 77 K using an ASAP2020 instrument. By utilizing the Barrett-Joyner-Halenda (BJH) model, the pore volumes and pore size distributions are got from the adsorption branches of isotherms. X-Ray photoelectron spectroscopy (XPS) studies are taken by a Perkin-Elmer PHI 5000CESCA system with Al K α radiation operated at 250 W. FTIR of the samples are recorded in transmission mode from KBr pellets at room temperature on a Bruker Tensor spectrometer with a resolution of 4 cm⁻¹, using 32 scans per spectrum in the region of 400–4000 cm⁻¹. The mass ratio of every sample to KBr is constant at 1 : 200. TG measurements of the catalysts are conducted on a Netzsch TG 209 F3 apparatus. The samples are placed in α -Al₂O₃ crucibles and heat in flowing argon gas (20 mL min⁻¹) from room temperature to 800 °C at a rate of 10 °C min⁻¹. The analysis of photoluminescence spectra (PL) and time resolved PL decay spectra is carried out at room temperature using a PTI QM-4 fluorescence spectrophotometer. Electrochemical Impedance Spectroscopy (EIS) are carried on the classical three-electrode system, using Zahner electrochemical station to test the electrochemical property of the samples. The supporting electrolyte is the mixed solution of 25 mmol L⁻¹ K₃Fe(CN)₆ and K₄Fe(CN)₃ and 0.1 mol L⁻¹ KCl. The counter, reference and working electrode are Pt electrode, saturated calomel electrode (SCE) and FTO glass coated with thin film sample, respectively. The electrode potential is 0.2 V *versus* SCE. The frequency range is from 0.1 to 10⁶ Hz.

2.6 Photocatalytic activity test

Photodegradation of a phenol solution (10 mg L⁻¹) is performed to evaluate the photocatalytic performance of the synthesized catalysts. The catalyst (50 mg) is added into the phenol solution (50 mL). Prior to irradiation, the suspension has a dark adsorption for half an hour. Then it was irradiated by a 300 W Xe lamp with a 420 nm cut off filter. At given time intervals, aliquots of the irradiated suspension are collected, centrifuged and analyzed by a HPLC system. In details, the aliquots were analyzed using "SHIMADZU LC-20A" which set with a two-channel UV-vis light absorption detector set at 270 nm absorbance for phenol detection. A Inertsil ODS-3 4.6 mm \times 150 mm \times 5 μ m C18 column was used, injected volume 10 μ L, column temperature of 40 °C and a flow of mobile phase acetonitrile: water (20 : 80, v/v) at a flow rate of 1.0 mL min⁻¹.

3. Results and discussion

3.1 Characterization results

XRD measurement. Fig. 1 Shows the wide-angle XRD patterns of CD-SBA15, 1 : 6 SBA15-CN and CD-SBA15-CN



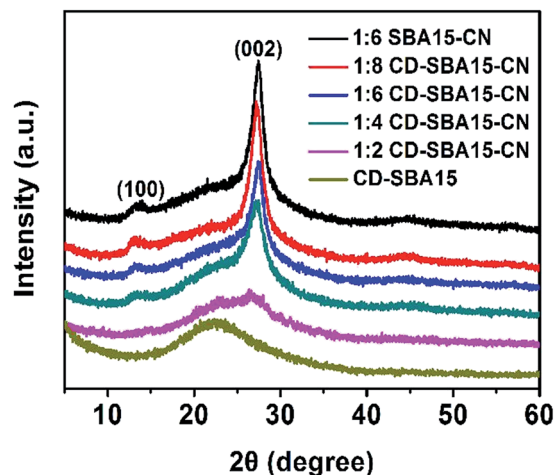


Fig. 1 Wide-angle XRD patterns of different samples.

photocatalysts. As can be seen from the figure, a broad peak at 22° which is attributed to amorphous silica is shown.²⁷ Compare with the diffraction peaks of CD-SBA15, two distinct peaks located at 13.1° and 27.4° are shown and the characteristic peak intensity of composites is stronger and stronger with increasing melamine amounts. The two peaks are indexed to the (100) and (002) diffraction planes of $g\text{-C}_3\text{N}_4$ and correspond to the interlayer stacking peak of aromatic systems and the in-plane structural packing motif of tri-s-triazine units.^{28,29} These two peaks together prove the successful synthesis of carbon nitride in the composite catalysts.

The N_2 adsorption-desorption measurement. The N_2 adsorption-desorption measurement is performed to explain characteristics of CD-SBA15 before and after coupling with carbon nitride. The isotherm of CD-SBA15 is of type IV in Fig. 2a according to the IUPAC classification, along with a steep H1 hysteresis loop in the range of $p/p^0 = 0.5\text{--}0.8$, indicating that the samples possessed typical mesoporous structures.^{30–32} Table 1 shows the structural features of the prepared catalysts. It is observed that SBA-15 has the largest BET surface area of $565.54\text{ m}^2\text{ g}^{-1}$ and the largest pore volume of $0.87\text{ cm}^3\text{ g}^{-1}$, while the CD-SBA15 shows a decrease in surface area and pore volume as CDs are loaded into the silica channel.

After the loading of $g\text{-C}_3\text{N}_4$, the mesoporous structure of all CD-SBA15- CN photocatalysts is maintained (Fig. 2b). As presented in Table 1, pure $g\text{-C}_3\text{N}_4$ has small specific surface area, small pore volume, and large pore size. After compositing CD-SBA15 or SBA-15 with $g\text{-C}_3\text{N}_4$, SBA15- CN and CD-SBA15- CN photocatalysts show relatively higher specific surface area, larger pore volume and smaller pore size as compared to the pure $g\text{-C}_3\text{N}_4$, but with increasing $g\text{-C}_3\text{N}_4$ amounts, the surface area, pore size and pore volume of the CD-SBA15- CN reduced, indicating the successful dispersed $g\text{-C}_3\text{N}_4$ into the pores of CD-SBA15 and existing an optimum content of $g\text{-C}_3\text{N}_4$.

TEM measurement. TEM is further used to confirm the mesoporous structure and the morphology of CD-SBA15 and CD-SBA15- CN photocatalysts. Fig. 3 shows the TEM images of SBA-15, 1 : 6 SBA15- CN , CD-SBA15 and 1 : 6 CD-SBA15- CN . As

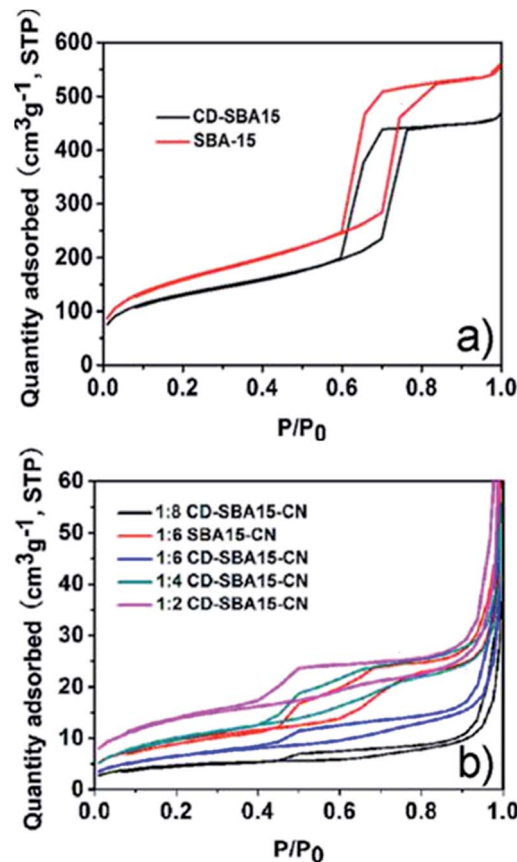


Fig. 2 N_2 adsorption-desorption isotherms of (a) SBA-15 and CD-SBA15, (b) CD-SBA15- CN series samples.

Table 1 Specific surface area, pore volume and pore size of $g\text{-C}_3\text{N}_4$, SBA-15, CD-SBA15 and CD-SBA15- CN photocatalysts

| Samples | S_{BET} ($\text{m}^2\text{ g}^{-1}$) | Pore volume ($\text{cm}^3\text{ g}^{-1}$) | Pore size (nm) |
|-----------------------------|----------------------------------------------------|------------------------------------------------|-------------------|
| $g\text{-C}_3\text{N}_4$ | 8.43 | 0.04 | 25.65 |
| SBA-15 | 565.54 | 0.87 | 5.65 |
| CD-SBA15 | 455.35 | 0.71 | 5.45 |
| 1 : 6 SBA15- CN | 38.11 | 0.10 | 3.80 |
| 1 : 2 CD-SBA15- CN | 47.58 | 0.15 | 3.99 |
| 1 : 4 CD-SBA15- CN | 36.47 | 0.09 | 3.81 |
| 1 : 6 CD-SBA15- CN | 23.35 | 0.08 | 3.79 |
| 1 : 8 CD-SBA15- CN | 16.05 | 0.05 | 3.69 |

shown in Fig. 3a and c, both SBA-15 and CD-SBA15 present highly ordered mesoporous structures, which are consistent with the N_2 adsorption-desorption isotherms (Fig. 2a). As for SBA15- CN in Fig. 3b and CD-SBA15- CN in Fig. 3d, the mesoporous have been partially filled with carbon nitride materials without obvious aggregation of carbon nitride observed and the hollow mesostructures are dominant, meaning the well dispersion of carbon nitride in CD-SBA15.

XPS analysis. XPS analysis can as a powerful evidence to show the composite catalyst is $g\text{-C}_3\text{N}_4$ loading into carbon dots modified SBA15, as it is widely used to investigate the chemical



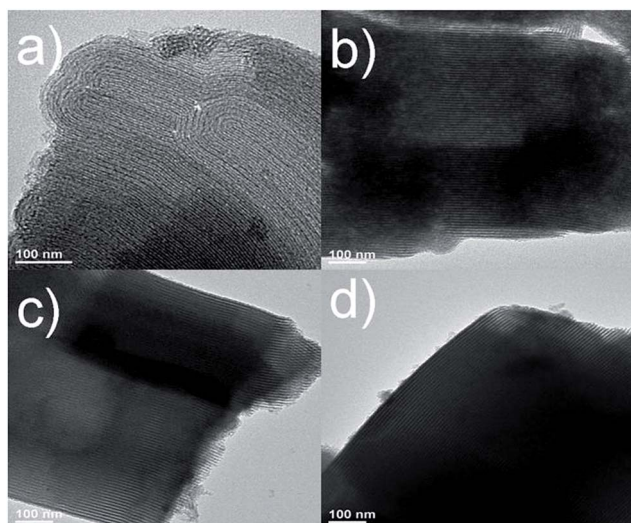


Fig. 3 TEM images of (a) SBA15, (b) 1 : 6 SBA15-CN, (c) CD-SBA15, (d) 1 : 6 CD-SBA15-CN.

composition of materials surface. Fig. 4a shows the survey spectrum of 1 : 6 CD-SBA15-CN, which reveals that elements of the sample including Si, O, C and N. As displayed in Fig. 4b, the high resolution spectrum of C 1s can be de-convoluted to three peaks at 288.5 eV, 288.3 eV and 284.8 eV. The peak at 284.8 eV corresponds to graphene carbon, and the weaker one at 288.3 eV is associated with sp^2 -bonded carbon (N-C=N) which usually appear in the XPS spectra of $g-C_3N_4$. In addition, the C 1s peak at 288.5 eV is identified as the bond of C=O.³³ This result coincides well with the high resolution spectrum of O 1s (Fig. 4d), in which the de-convoluted peaks around 535.2 eV and 531.6 eV corresponded to -OH and HO-C=O, respectively,³⁴ what have identified the existence of carbon dot. Besides, as we can see from the N 1s core level in Fig. 4c, the de-convoluted peak centered at 398.5 eV belong to sp^2 -hybridized nitrogen

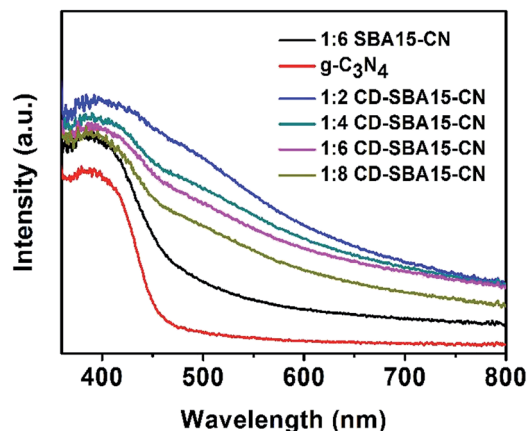


Fig. 5 UV-vis absorption spectra of different materials.

(C-N=C). And the peaks at 399.6 eV and 400.8 eV correspond to the nitrogen in N-(C)₃ and C-N-H which come from the $g-C_3N_4$, respectively.^{35,36} All above results further confirmed the formation of samples composed of $g-C_3N_4$ and carbon dots, suggesting the $g-C_3N_4$ have been introduced into the CD-SBA15 successfully.

UV-vis measurement. The optical absorption properties of the prepared CD-SBA15-CN composites are investigated by UV-vis diffuse reflectance spectroscopy. The results are shown in Fig. 5. It can be found that the absorption edge of $g-C_3N_4$ is about 450 nm. The red-shift of the absorption edge and the increase of the absorption intensity of 1 : 6 SBA15-CN in visible light region can also be observed. This indicates that the modification of SBA-15 can improve visible light utilization of SBA15-CN photocatalysts due to the high dispersion of $g-C_3N_4$ in SBA-15 channel. By contrast, the visible light harvesting capability of the CD-SBA15-CN composites increase with the decrease of $g-C_3N_4$ due to the intrinsic optical absorbance of the CDs, which indicates that CD-SBA15-CN can absorb more energy from the visible light that leads to enhance photocatalytic activity. A further observation is that the absorption edge of CD-SBA15-CN shift, which suggests the incorporation of CDs into the $g-C_3N_4$.

3.2 Photocatalytic performances

Photocatalytic degradation of phenol. To evaluate the visible light photocatalytic activity of the as-prepared samples, a test reaction is carried out for degradation of 10 mg L⁻¹ of phenol with 50 mg of the catalyst under visible light irradiation. And the results are shown in Fig. 6. It can be seen from Fig. 6, the degradation of phenol hardly occurs under visible light irradiation in the presence of CD-SBA15. Instead, the degradation of phenol proceeds obviously with $g-C_3N_4$. The phenol degradation rate of 1 : 6 SBA15-CN reaches 36%, which is 2 times as high as that of bare $g-C_3N_4$. After loading of CDs into the mesoporous channels of SBA-15, the phenol degradation rate can be further enhanced. In addition, by optimizing the mass ratio of CD-SBA15 to $g-C_3N_4$, the best photocatalytic performance of CD-SBA15-CN photocatalysts can be achieved for 1 : 6 CD-SBA15-CN, whose phenol degradation rate almost reaches 70%.

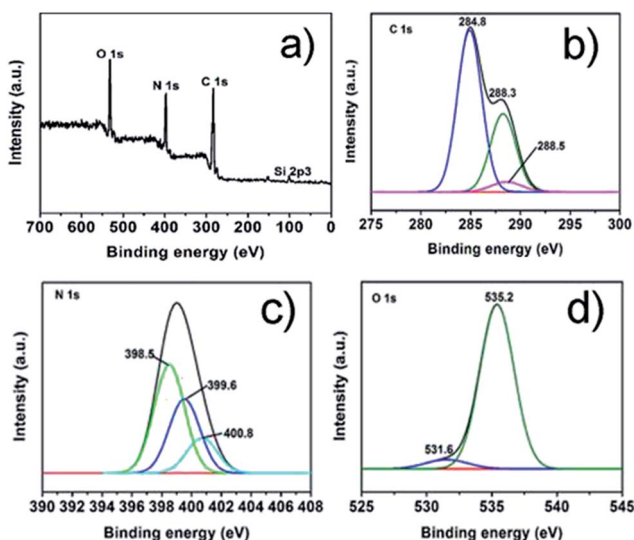


Fig. 4 XPS spectra of 1 : 6 CD-SBA15-CN: (a) survey scan; (b) deconvoluted C 1s; (c) deconvoluted N 1s and (d) deconvoluted O 1s.



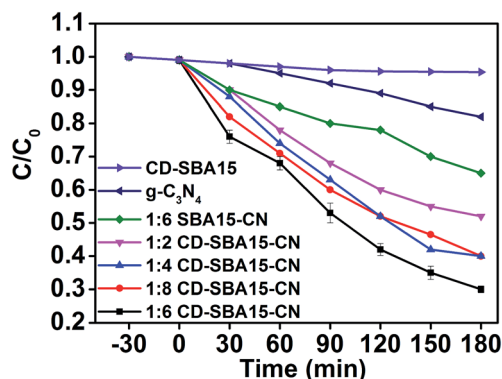


Fig. 6 Photocatalytic degradation of phenol (10 mg L^{-1}) over different materials under visible light irradiation ($\lambda > 420 \text{ nm}$).

Photocatalytic mechanism. To investigate the mechanism for the enhancement of the photocatalytic activity by combining $\text{g-C}_3\text{N}_4$ and CDs in SBA-15, photoluminescence (PL) spectra are measured, which are shown in Fig. 7. For CD-SBA15, there is an intense emission come from the loading carbon dots. The pristine $\text{g-C}_3\text{N}_4$ exhibits a strong emission centered at 460 nm. This emission results from the radiative recombination of the photo-generated charge carriers in $\text{g-C}_3\text{N}_4$. Obviously, the 1 : 6 SBA15-CN shows weaker emission intensity than that of $\text{g-C}_3\text{N}_4$. The significant PL quenching of $\text{g-C}_3\text{N}_4$ may be because of the well dispersion of $\text{g-C}_3\text{N}_4$ fragments with decreased particle size in the SBA-15 channels, shortening the transfer distance of the photo-generated charge carriers to the active sites on the surface and consequently effectively promoting the separation of the photo-generated charge carriers in 1 : 6 SBA15-CN. For 1 : 6 CD-SBA15-CN, the PL intensity is further decreased, indicating the interaction between CDs and $\text{g-C}_3\text{N}_4$ can promote the separation of charges more effectively,^{37–39} which is consistent with the photocatalytic activity of the samples.

Besides the PL measurement, electrochemical impedance spectroscopy (EIS) is another important measurement to investigate the charge transfer ability of the catalysts.^{40–42} A smaller arc radius means a higher utilization of visible light and a higher photocatalytic activity. As shown in Fig. 8 as we can see that $\text{g-C}_3\text{N}_4$ has the largest arc radius, suggesting a high charge transport resistance of the material. After $\text{g-C}_3\text{N}_4$ loading on SBA-15, high disperse $\text{g-C}_3\text{N}_4$ has a smaller charge transport

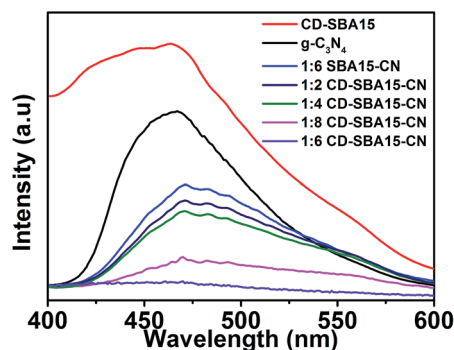


Fig. 7 PL emission spectra of different samples.

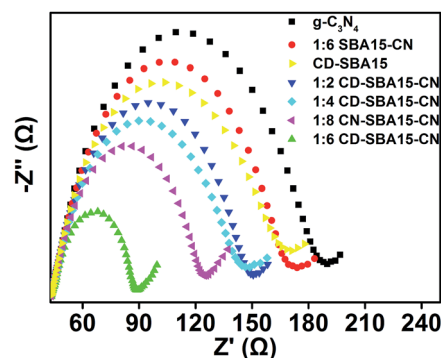


Fig. 8 Electrochemical impedance spectroscopy of different samples.

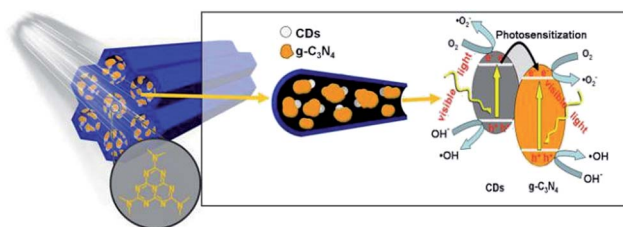


Fig. 9 The proposed photocatalytic mechanism of CD-SBA15-CN composites.

resistance, which means a more quickly transfer photo-generated electrons. When the carbon dots combine with SBA15, carbon dots can quickly transfer photogenerated electrons (that's why CD-SBA15 has a smaller arc radius) showed a much smaller arc radius. As a result, compare with SBA15-CN, arc radius of CD-SBA15-CN is smaller, and 1 : 6 CD-SBA15-CN is smallest, which means photogenerated electrons on 1 : 6 CD-SBA15-CN can be quickly transferred then have an excellent photocatalytic performance.

Based on the above results, a mechanism for the enhanced photocatalytic phenol degradation and charge transfer over the CD-SBA15-CN composite photocatalyst is proposed and schematically illustrated in Fig. 9. The high dispersion of $\text{g-C}_3\text{N}_4$ into CD-SBA15 leads to reduced recombination of photo-generated electrons and holes, as proved by the PL analysis. In addition, the combination of $\text{g-C}_3\text{N}_4$ and CDs in the mesoporous can make the catalyst absorb more visible light, resulting in more photo-generated electrons and holes. Moreover, CDs could inject electrons to $\text{g-C}_3\text{N}_4$ under visible light irradiation, serving as photosensitizer to $\text{g-C}_3\text{N}_4$.⁴³ Lastly, the interaction between CDs and $\text{g-C}_3\text{N}_4$ could help the photogenerated electrons transfer more efficiently as demonstrated by the EIS result, further reduce the recombination rate of electron-hole pairs as well as greatly promote the generation of active species on the surface. Collectively, all the above contributed to the enhanced photocatalytic activity, accelerated the phenol degradation.

Conclusion

To sum up, $\text{g-C}_3\text{N}_4$ has been successfully loaded into the CD-SBA15 by an impregnation method. The obtained SBA15-CN



composites exhibit better photocatalytic performance than the pure g-C₃N₄ under visible light irradiation. The well dispersion of g-C₃N₄ into SBA-15 can shorten the distance for charge transfer and inhibit the recombination of charges in g-C₃N₄. Moreover, for CD-SBA15-CN, the photocatalytic activity under visible light is further improved because the CDs can enhance the adsorption of visible light and the interaction between CDs and g-C₃N₄ can promote the separation of photo-generated electron-hole pairs. This thought of charge transfer enhancement by the CD-SBA15 will provide a new route to develop advanced composite catalysts for water purification.

Conflicts of interest

There are no conflicts to declare.

Acknowledgements

This work was financially supported by National Nature Science Foundation of China (21407049, 21377038, 21237003, 21677048), Science and Technology Commission of Shanghai Municipality (16JC1401400, 17520711500), National Key Research and Development Program (2016YFA0204200), China Postdoctoral Science Foundation (2015T8049), the Fundamental Research Funds for the Central Universities (222201714061).

Notes and references

- 1 C. Chen, W. Ma and J. Zhao, *Chem. Soc. Rev.*, 2010, **39**, 4206.
- 2 J. Schneider, M. Matsuoka, M. Takeuchi, J. Zhang, Y. Horiuchi, M. Anpo and D. W. Bahnemann, *Chem. Rev.*, 2014, **114**, 9919.
- 3 H. Li, X. Shen, Y. D. Liu, L. Z. Wang, J. Y. Lei and J. L. Zhang, *J. Alloys Compd.*, 2015, **646**, 380–386.
- 4 H. Li, L. Zhou, L. Z. Wang, Y. D. Liu, J. Lei and J. L. Zhang, *Phys. Chem. Chem. Phys.*, 2015, **17**, 17406–17412.
- 5 Y. Liu, P. Zhang, B. Z. Tian and J. L. Zhang, *ACS Appl. Mater. Interfaces*, 2015, **7**, 13849.
- 6 Y. Liu, P. Zhang, B. Z. Tian and J. L. Zhang, *Catal. Commun.*, 2015, **70**, 30.
- 7 J. Y. Lei, Y. Chen, F. Shen, L. Z. Wang, Y. D. Liu and J. L. Zhang, *J. Alloys Compd.*, 2015, **631**, 328.
- 8 H. Li, L. Z. Wang, Y. D. Liu, J. Y. Lei and J. L. Zhang, *Res. Chem. Intermed.*, 2016, **42**, 3979.
- 9 X. C. Wang, K. Maeda, A. Thomas, K. Takanabe, G. Xin, J. M. Carlsson, K. Domen and M. Antonietti, *Nat. Mater.*, 2009, **8**, 76.
- 10 D. Masih, Y. Ma and S. Rohani, *Appl. Catal., B*, 2017, **206**, 556.
- 11 Y. M. Liu, J. P. Wang and P. Yang, *RSC Adv.*, 2016, **6**, 34334.
- 12 Z. W. Zhao, Y. J. Sun and F. Dong, *Nanoscale*, 2015, **7**, 15.
- 13 S. Patnaik, S. Martha and K. M. Parida, *RSC Adv.*, 2016, **52**, 46929.
- 14 W. Iqbal, B. C. Qiu, J. Y. Lei, L. Z. Wang, J. L. Zhang and M. Anpo, *Dalton Trans.*, 2017, **46**, 10678–10684.
- 15 L. Zhou, L. Z. Wang, J. Y. Lei, Y. D. Liu and J. L. Zhang, *Catal. Commun.*, 2017, **89**, 125.
- 16 J. Y. Lei, F. H. Liu, L. Z. Wang, Y. D. Liu and J. L. Zhang, *RSC Adv.*, 2017, **7**, 27377.
- 17 L. Zhou, L. Z. Wang, J. L. Zhang, J. Y. Lei and Y. D. Liu, *Eur. J. Inorg. Chem.*, 2016, **34**, 5387.
- 18 H. Zhang, L. X. Zhao, F. L. Geng, L. H. Guo, B. Wan and Y. Yang, *Appl. Catal., B*, 2016, **180**, 656.
- 19 S. Shen and L. Guo, *Mater. Res. Bull.*, 2008, **43**, 437.
- 20 Z. Huang, F. B. Li, B. F. Chen, T. Lu, Y. Yuan and G. Q. Yuan, *Appl. Catal., B*, 2013, **136**, 269.
- 21 C. Cheng, X. J. Tan and J. Zhang, *Chem.–Eur. J.*, 2015, **21**, 17944.
- 22 F. Wang, Z. Xie, H. Zhang, C. Y. Liu and Y. G. Zhang, *Adv. Funct. Mater.*, 2011, **21**, 1027.
- 23 J. Y. Lei, L. G. Yang, X. F. Yan, C. Cheng, Y. D. Liu, L. Z. Wang and J. L. Zhang, *Adv. Opt. Mater.*, 2015, **3**, 57.
- 24 L. G. Wang, C. Cheng, S. Tapas, J. Y. Lei, M. Matsuoka, J. L. Zhang and F. Zhang, *J. Mater. Chem. A*, 2015, **3**, 13357.
- 25 C. Cheng, X. J. Tan, D. Lu, L. Z. Wang, T. Sen, J. Y. Lei, A. M. El-Toni, J. L. Zhang, F. Zhang and D. Zhao, *Chem.–Eur. J.*, 2015, **21**, 17944.
- 26 D. Y. Zhao, J. L. Feng, Q. S. Huo, N. Melosh, G. H. Fredrickson, B. F. Chmelka and G. D. Stucky, *Science*, 1998, **279**, 548.
- 27 D. Y. Zhao, Q. S. Huo, J. L. Feng, B. F. Chmelka and G. D. Stucky, *J. Am. Chem. Soc.*, 1998, **120**, 6024.
- 28 Y. M. Wu, L. Tao, J. Zhao, X. Yue, W. Y. Deng, Y. X. Li and C. Y. Wang, *Res. Chem. Intermed.*, 2016, **42**, 3609.
- 29 C. Z. Zhu, Z. F. Jiang, W. Wei, L. L. Chen, D. Liu, K. Qian, X. M. Lu and J. M. Xie, *Res. Chem. Intermed.*, 2016, **42**, 6483.
- 30 J. Y. Lei, L. G. Yang, D. Lu, X. F. Yan, C. Cheng, Y. D. Liu, L. Z. Wang and J. L. Zhang, *Adv. Opt. Mater.*, 2015, **3**, 57–63.
- 31 J. Y. Lei, L. Z. Wang and J. Zhang, *ACS Nano*, 2011, **5**, 3447.
- 32 J. Lei, L. Wang and J. Zhang, *Chem. Commun.*, 2010, **46**, 8445.
- 33 Y. Wu, M. Xing and J. Zhang, *J. Hazard. Mater.*, 2011, **192**, 368.
- 34 J. Mao, T. Peng, X. Zhang, K. Li, L. Ye and L. Zan, *Catal. Sci. Technol.*, 2013, **3**, 1253.
- 35 X. Lu, K. Xu, P. Chen, K. Jia, S. Liu and C. Wu, *J. Mater. Chem. A*, 2014, **2**, 18924.
- 36 Y. Hou, Z. Wen, S. Cui, X. Guo and J. Chen, *Adv. Mater.*, 2013, **25**, 6291.
- 37 B. Subash, B. Krishnakumar, M. Swaminathan and M. Shanthi, *Res. Chem. Intermed.*, 2013, **39**, 3181.
- 38 F. H. Liu, J. Yu, G. Y. Tu, L. Qu, J. C. Xiao, Y. D. Liu, L. Z. Wang, J. Lei and J. L. Zhang, *Appl. Catal., B*, 2017, **201**, 1.
- 39 X. F. Wang, J. J. Cheng, H. G. Yu and J. G. Yu, *Catal. Sci. Technol.*, 2013, **1**.
- 40 M. Chen, L. L. Shao, Y. X. Guo and X. Q. Cao, *Chem. Eng. J.*, 2016, **304**, 303.
- 41 X. Liu, L. J. Chen, R. Y. Chen, Z. Chen, X. Chen and X. Zheng, *Res. Chem. Intermed.*, 2015, **41**, 3623.
- 42 S. M. Yin, J. Y. Han, T. H. Zhou and R. Xu, *Catal. Sci. Technol.*, 2015, **5**, 5048.
- 43 J. C. Bian, C. Huang, L. Y. Wang, T. F. Hung, A. W. Daoud and R. Q. Zhang, *ACS Appl. Mater. Interfaces*, 2014, **6**, 4883.

